Constraints from High Redshift Supernovae upon Scalar Field Cosmologies

Joshua A. Frieman
NASA/Fermilab Astrophysics Center, Fermi National Accelerator Laboratory
PO Box 500, Batavia IL 60510, USA
Department of Astronomy and Astrophysics
University of Chicago, Chicago, IL 60637 USA

Ioav Waga
Universidade Federal do Rio de Janeiro, Instituto de Física
Rio de Janeiro, RJ, 21945-970, Brazil
(February 1, 2008)

Recent observations of high-redshift Type Ia supernovae have placed stringent constraints on the cosmological constant Λ. We explore the implications of these SNe observations for cosmological models in which a classically evolving scalar field currently dominates the energy density of the Universe. Such models have been shown to share the advantages of Λ models: compatibility with the spatial flatness predicted inflation; a Universe older than the standard Einstein-de Sitter model; and, combined with cold dark matter, predictions for large-scale structure formation in good agreement with data from galaxy surveys. Compared to the cosmological constant, these scalar field models are consistent with the SNe observations for a lower matter density, $\Omega_{m0} \sim 0.2$, and a higher age, $H_0 t_0 \gtrsim 1$. Combined with the fact that scalar field models imprint a distinctive signature on the cosmic microwave background anisotropy, they remain currently viable and should be testable in the near future.

98.80.Cq

I. INTRODUCTION

In recent years, models with a relic cosmological constant Λ have received considerable attention for a number of reasons. First, dynamical estimates of the mass density on the scales of galaxy clusters suggest that $\Omega_m = 0.2 \pm 0.1$ for the matter m that clusters gravitationally (where $\Omega(t)$ is the ratio of the mean mass density of the universe to the critical Einstein-de Sitter density, $\Omega(t) = 8\pi G\rho/3H^2$) [1]. (Some density estimates on larger scales are higher but remain controversial [2].) However, if a sufficiently long epoch of inflation took place during the early universe, the present spatial curvature should be negligibly small, $\Omega_{tot} = 1$. A cosmological constant, with effective density parameter $\Omega_\Lambda \equiv \Lambda/3H_0^2 = 1 - \Omega_m$, is one way to resolve the discrepancy between Ω_m and Ω_{tot}.

The second motivation for the revival of the cosmological constant has been the 'age crisis' for spatially flat $\Omega_m = 1$ models, though the evidence currently is more ambiguous than it was. Estimates of the Hubble expansion parameter from a variety of methods are converging to $h \equiv (H_0/100 \text{ km/sec/Mpc}) = 0.7 \pm 0.1$ [3], while determinations of the age of the universe from globular clusters have typically been in the range $t_{gc} \simeq 13 - 15$ Gyr or higher [4]. These observations imply a value for the 'expansion age', $H_0 t_0 = (H_0/70 \text{ km/sec/Mpc})(t_0/14 \text{ Gyr}) \simeq 1.0 \pm 0.2$, higher than that for the standard Einstein-de Sitter model, for which $H_0 t_0 = 2/3$. On the other hand, for models with a cosmological constant, $H_0 t_0$ can be larger: for example, for $\Omega_\Lambda = 0.75 = 1 - \Omega_m$, one finds $H_0 t_0 = 1.0$. This argument has recently been called into question, however: revised determinations of t_{gc} based on the Hipparcos distance scale are lower by approximately 2 Gyr [5]. If confirmed, this would largely alleviate the age problem.

Third, cosmological constant-dominated models for large-scale structure formation with cold dark matter (CDM) and a nearly scale-invariant spectrum of primordial density perturbations (as predicted by inflation) provide a better fit to the observed power spectrum of galaxy clustering than does the 'standard' $\Omega_m = 1$ CDM model [6]. In particular, the shape of the power spectrum of galaxy surveys is generally consistent with $\Gamma = \Omega_m h = 0.25 \pm 0.05$ [7].

Despite these successes, cosmological constant models face several difficulties of their own. On aesthetic grounds, it is difficult to understand why the vacuum energy density of the universe, $\rho_\Lambda \equiv \Lambda m_{Pl}^2/8\pi$, should be of order $(10^{-3}\text{eV})^4$, as it must be to have a cosmological impact ($\Omega_\Lambda \sim 1$). On dimensional grounds, one would expect it to be many orders of magnitude larger – of order m_{Pl}^4 or perhaps m_{SUSY}^4. Since this is not the case, we might plausibly assume that some physical mechanism sets the ultimate vacuum energy to zero. Why then is it not zero today?

In addition, the cosmological constant now faces strong observational challenges. In Λ models, a larger fraction of distant QSOs would be gravitationally lensed than in a $\Lambda = 0$ universe; surveys for lensed QSOs have been used to infer the bound $\Omega_\Lambda < 0.66$ at 95 % C.L. [8]. Further, while the power spectra of Λ models with CDM have approximately

the right shape to fit the galaxy clustering data, the COBE-normalized amplitude is too high, requiring galaxies to be anti-biased relative to the mass distribution [9].

Motivated by these theoretical and observational difficulties of the cosmological constant, attention has turned to models in which the energy density resides in a dynamical scalar field rather than in a pure vacuum state. These *dynamical* Λ models [10–13] were proposed in response to the aesthetic difficulties of cosmological constant models. They were found to partially alleviate their observational problems as well; for example, the statistics of gravitationally lensed QSOs yields a less restrictive upper bound on $H_0 t_0$ in these models [13–15]. In addition, for a range of model parameters, the amplitude of the density power spectrum is reduced relative to that of ΛCDM while its shape is retained [16]. These models also have a signature in the cosmic microwave background (CMB) temperature anisotropy angular power spectrum that is distinctive from Λ and Einstein-de Sitter models [16,17]. Consequently, they should be tested with the next generation of high-resolution CMB temperature maps, e.g., from the MAP and Planck satellite missions.

In this paper, we consider another set of observational constraints on these cosmological models, arising from high-redshift supernovae. On-going projects to discover Type Ia supernovae at redshifts $z \sim 0.3 - 1$, coupled with improved techniques to narrow the dispersion in SN Ia peak magnitudes, have renewed the prospects for determining the cosmological parameters [19,20]. Based on analysis of an initial set of 7 high-redshift SNe Ia, Perlmutter etal. obtained the bound $\Omega_\Lambda < 0.51$ at 95% C.L. [19] for spatially flat cosmological constant models. For Λ models, this implies $H_0 t_0 < 0.84$ at this limit. These are preliminary results from a new method; the degree to which they are affected by evolution, absorption, etc., will be determined by the much larger samples now being gathered (the world sample of high-redshift SNe is now roughly a factor of 10 larger than that used to obtain the bound above).

We consider constraints on dynamical scalar field models arising from high-redshift SNe Ia observations and compare them with constraints on Λ models. The SNe Ia implications for some different but related cosmological models–in which there is an extra component described by an arbitrary fixed equation of state–have recently been studied in Refs. [21]. Here, we focus on three representative models for 'ultra-light' scalar fields: pseudo-Nambu-Goldstone bosons (PNBGs) [13], inverse-power-law potentials [11], and exponential potentials. In §II, we review the motivation for and cosmic evolution of these models. In §III, we derive the corresponding constraints from the SNe observations. We conclude in §IV.

II. SCALAR FIELD COSMOLOGICAL MODELS

The classical action for a scalar field ϕ has the form

$$S = \frac{m_{Pl}^2}{16\pi} \int d^4x \sqrt{-g} \left[\left(-R + \frac{1}{2} g^{\mu\nu} \partial_\mu \phi \partial_\nu \phi - V(\phi) \right) + \mathcal{L} \right], \tag{2.1}$$

where $m_{Pl} = G^{-1/2}$ is the Planck mass, R is the Ricci scalar, $g \equiv \det g_{\mu\nu}$, $V(\phi)$ is the scalar field potential, and $\mathcal{L}$ is the Lagrangian density of non-relativistic matter and radiation. For simplicity, we assume ϕ is minimally coupled to the curvature, and we work in units in which $\hbar = c = 1$. We consider spatially flat, homogenous and isotropic cosmologies described by the line element

$$ds^2 = dt^2 - a^2(t) \left(dx^2 + dy^2 + dz^2 \right) \ , \tag{2.2}$$

where $a(t)$ is the Friedmann-Robertson-Walker (FRW) scale factor.

In this paper, we focus on models in which the scalar field is dynamically important only at relatively recent epochs, at redshifts $z \lesssim 10$. Thus, we model the matter content of the Universe as a two-component system comprising the scalar field ϕ and non-relativistic matter m. Further, we assume that the energy-momentum of each component is separately conserved, so the matter energy density scales as $\rho_m \propto a^{-3}$. (There is no particle production as in some decaying Λ models proposed in the literature [10].)

The Einstein and scalar field equations can be written as:

$$\frac{dH}{dt} + \frac{3}{2} H^2 + \frac{2\pi}{m_{Pl}^2} \left(\frac{d\phi}{dt} \right)^2 - \frac{4\pi}{m_{Pl}^2} V(\phi) = 0, \tag{2.3}$$

$$\frac{d^2\phi}{dt^2} + 3H \frac{d\phi}{dt} + \frac{dV}{d\phi} = 0 \tag{2.4}$$

where the Hubble parameter

$$H^2 = \left(\frac{1}{a}\frac{da}{dt}\right)^2 = \frac{8\pi}{3m_{Pl}^2}\left[\frac{1}{2}\left(\frac{d\phi}{dt}\right)^2 + V(\phi) + \rho_m\right] \ . \tag{2.5}$$

In what follows, it will also be useful to characterize the instantaneous equation of state of the scalar field by defining its effective adiabatic index,

$$\gamma_\phi(t) = 1 + \frac{p_\phi}{\rho_\phi} = \frac{2\left(\frac{d\phi}{dt}\right)^2}{\left(\frac{d\phi}{dt}\right)^2 + 2V(\phi)} \ . \tag{2.6}$$

For a static field, corresponding to a cosmological constant Λ, $\gamma_\Lambda = 0$, while for pressureless dust, $\gamma = 1$.

A number of models with a dynamical Λ have been discussed in the literature [10–13]. We consider three representative scalar field potentials that give rise to effective decaying Λ models.

A. The PNGB model

Consider the properties that a massive scalar field must satisfy in order to act approximately like a cosmological constant at recent epochs. Vacuum energy is stored in the potential energy density $V(\phi) \sim M^4$, where M sets the characteristic height of the potential, and we set $V(\phi_m) = 0$ at the minimum of the potential by the assumption that the fundamental vacuum energy of the Universe is zero (for reasons not yet understood). In order to generate a non-zero Λ at the present epoch, ϕ must initially be displaced from the minimum ($\phi_i \neq \phi_m$ as an initial condition), and its kinetic energy must be relatively small compared to its potential energy. This implies that the motion of the field is still (nearly) overdamped, so the scalar mass must be extremely small, $m_\phi \equiv \sqrt{|V''(\phi_i)|} \lesssim 3H_0 = 5 \times 10^{-33} h$ eV. In addition, for $\Omega_\phi \sim 1$, the potential energy density should be of order the critical density, $M^4 \sim 3H_0^2 m_{Pl}^2/8\pi$, or $M \simeq 3 \times 10^{-3} h^{1/2}$ eV. Thus, the characteristic height and curvature of the potential are strongly constrained for a classical model of the cosmological constant.

In quantum field theory, such ultra-low-mass scalars are not *generically* natural: radiative corrections generate large mass renormalizations at each order of perturbation theory. To incorporate ultra-light scalars into particle physics, their small masses should be at least 'technically' natural, that is, protected by symmetries, such that when the small masses are set to zero, they cannot be generated in any order of perturbation theory, owing to the restrictive symmetry.

From the viewpoint of quantum field theory, pseudo-Nambu-Goldstone bosons (PNGBs) are the simplest way to have naturally ultra–low mass, spin–0 particles. PNGB models are characterized by two mass scales, a spontaneous symmetry breaking scale f (at which the effective Lagrangian still retains the symmetry) and an explicit breaking scale M (at which the effective Lagrangian contains the explicit symmetry breaking term). The PNGB mass is then $m_\phi \sim M^2/f$. Thus, the two dynamical conditions on m_ϕ and M above essentially fix these two mass scales to be $M \sim 10^{-3}$ eV, interestingly close to the neutrino mass scale for the MSW solution to the solar neutrino problem, and $f \sim m_{Pl} \simeq 10^{19}$ GeV, the Planck scale. Since these scales have a plausible origin in particle physics models, we may have an explanation for the 'coincidence' that the vacuum energy is dynamically important at the present epoch [13,22,23]. Moreover, the small mass m_ϕ is technically natural.

The effective scalar field potential in PNGB models is approximated by

$$V(\phi) = M^4\left(1 + \cos\left(\phi/f\right)\right) \ . \tag{2.7}$$

Constraints on the $f - M$ parameter space from gravitational lensing were analyzed in [13]; the large-scale power spectrum and CMB anistropy for these models were studied in [16–18].

To numerically integrate the field equations, we define dimensionless variables,

$$u = \frac{1}{H_0 f}\frac{d\phi}{dt}, \ v = \frac{H}{H_0} \quad \text{and} \quad w = \frac{\phi}{f}. \tag{2.8}$$

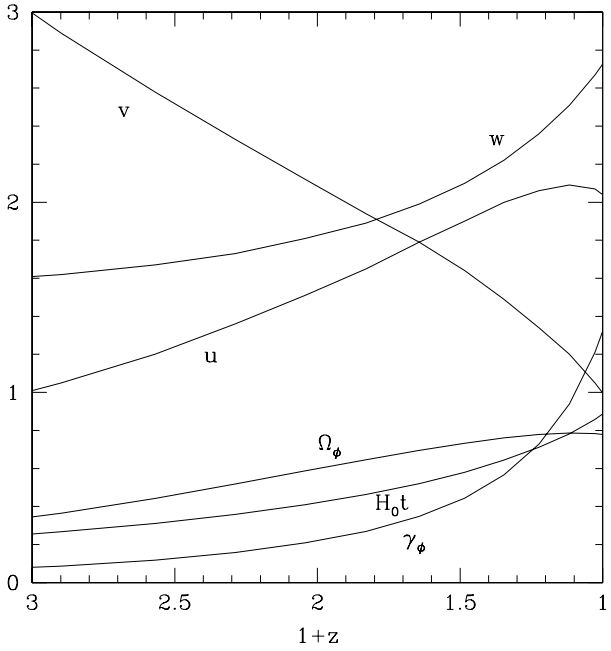

FIG. 1. The quantities u, v, w, Ω_ϕ, $H_0 t$, and γ_ϕ as a function of redshift for the PNGB model with $f = 2.07 \times 10^{18}$ GeV and $M = 0.004 h^{1/2}$ eV. The initial field conditions are chosen to be $w_i = \phi_i/f = 1.5$, $u_i = 0$.

With these definitions, we can rewrite the equations of motion in first order form,

$$\dot{w} = u, \tag{2.9}$$

$$\dot{u} + 3uv - \frac{M^4}{H_0^2 f^2} \sin w = 0, \tag{2.10}$$

$$\dot{v} + \frac{3}{2}v^2 + \frac{2\pi f^2}{m_{Pl}^2}u^2 - \frac{4\pi M^4}{m_{Pl}^2 H_0^2}\,(1 + \cos w) = 0. \tag{2.11}$$

Here the overdot denotes $(1/H_0)d/dt$. We numerically solve the above equations assuming that $u(t_i) = 0$ and that $v(t_i) \gg 1$ (so the universe is initially matter-dominated).

In Fig. 1 we show the quantities u, v, w, Ω_ϕ, $H_0 t$, and γ_ϕ as a function of redshift, $1+z = a_0/a(t)$, for the parameters $f = 2.07 \times 10^{18}$ GeV and $M = 0.004 h^{1/2}$ eV. The initial conditions for the field were taken to be $w_i = \phi_i/f = 1.5$, $u_i = 0$. For this choice of parameters and initial conditions, $\Omega_{\phi 0} = 0.78$ and $H_0 t_0 = 0.89$. (For comparison, for a Λ model with $\Omega_\Lambda = 0.78$, we would have $H_0 t_0 = 1.05$; in an open model with the same value of $\Omega_{m0} = 0.22$, the corresponding age is $H_0 t_0 = 0.84$.) The u and w curves indicate that the field is just beginning to decelerate at redshift $z \simeq 0.1$, as it nears the potential minimum ($w_m = \pi$) for the first time. At high redshift, when the field is nearly static, the adiabatic index $\gamma_\phi \simeq 0$, and the field acts as a pure cosmological constant; at late times, when the field kinetic energy becomes appreciable, γ rises above unity. In the future, the field would undergo damped oscillations around the minimum at $w = \pi$, and γ would settle down to unity, the value for pressureless dust.

In Figs. 2 and 3, we plot contours of $\Omega_{\phi 0}$ and $H_0 t_0$ as a function of the parameters f and M, also for $w_i = \phi_i/f = 1.5$. (For different choices of w_i, the contour levels would shift around in the $f - M$ plane; for comparison, see [13,16].) These figures show that there is a range of model parameters which give rise to acceptable values of $\Omega_{\phi 0}$ and $H_0 t_0$. We also note that, in the region of parameter space studied here, the linear transfer function for the growth of large-scale structure has an effective shape parameter given by $\Gamma = (1 - \Omega_{\phi 0})h$, but the perturbation amplitude can differ from that in the corresponding Λ model [16].

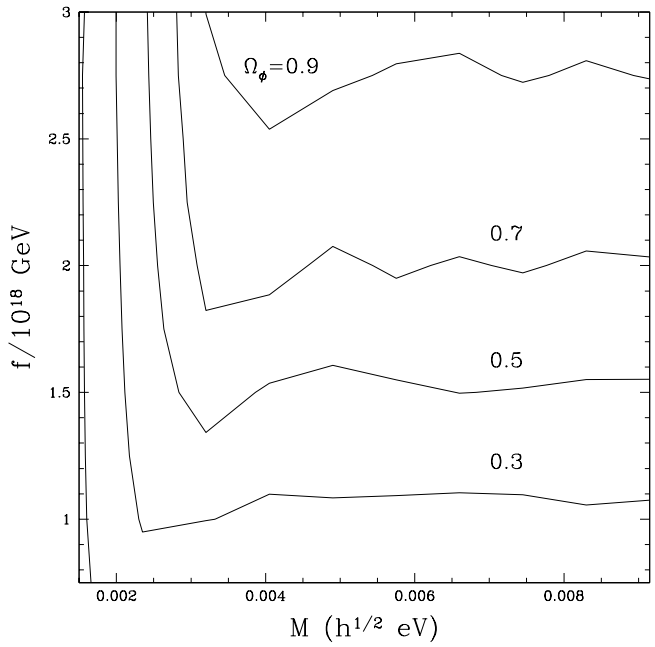

FIG. 2. Contours of constant $\Omega_{\phi 0}$ in the $f - M$ plane for the PNGB model, with $w_i = 1.5$.

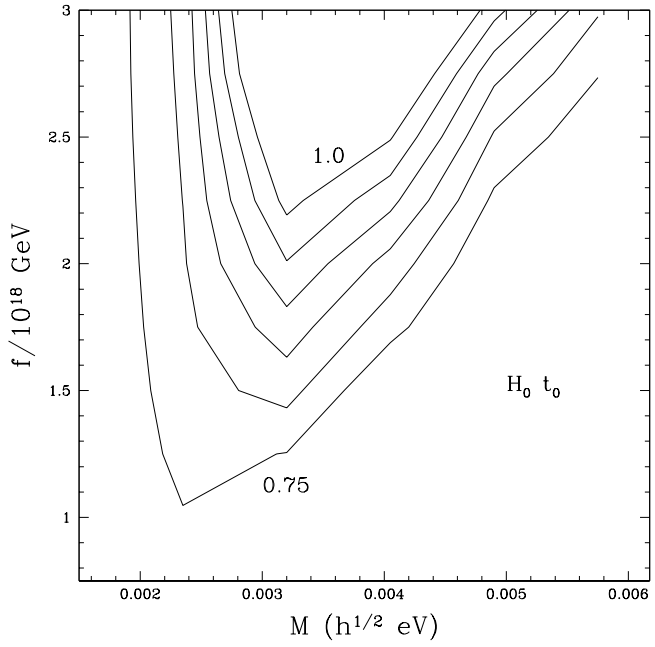

FIG. 3. Contours of constant $H_0 t_0$ in the $f - M$ plane for the PNGB model, with $w_i = 1.5$.

B. Power-law potentials

For these models the scalar field potential has the form of an inverse power-law,

$$V(\phi) = \frac{k}{32\pi} m_{Pl}^4 \left(\frac{m_{Pl}}{\sqrt{16\pi}\phi} \right)^\alpha \ , \tag{2.12}$$

where $k > 0$ and $\alpha > 0$ are dimensionless constants. Scalar potentials of this form arise, e.g., in dynamically broken supersymmetry theories in which flat directions are lifted by non-perturbative effects [24]. However, for such a field to be dynamically relevant today requires $k \sim 10^{-120}$; this is just another statement of the cosmological constant problem.

Cosmological consequences of scalar fields with such a potential were investigated in [11,12,14]. For $\alpha \to 0$, the scalar field energy-momentum tensor approaches that of a conventional cosmological constant Λ, i.e., $\rho_\phi =$ constant; in the opposite limit $\alpha \to \infty$, the scalar field energy density scales like that of non-relativistic matter, $\rho_\phi \propto a^{-3}$. More generally, in the matter-dominated era at $z \gg 1$, when $\rho_\phi \ll \rho_m$, the scalar field energy density scales as $\rho_\phi \propto a^{-3\alpha/(\alpha+2)}$. Thus, for fixed $\Omega_{\phi 0}$, the angular diameter distance to a fixed redshift, and thus the optical depth for gravitational lensing, decreases as α increases. Unlike the case of a cosmological constant, in these models it is possible to satisfy the lensing constraints [8] even for low values of Ω_{m0} (see Ref. [14]). As we shall see in the next section, similar statements apply for the high redshift supernovae constraints.

By defining dimensionless variables,

$$u = \frac{4\sqrt{\pi}}{H_0 m_{Pl}} \frac{d\phi}{dt}, \ v = \frac{H}{H_0}, \text{ and } w = \frac{4\sqrt{\pi}\phi}{m_{Pl}}. \tag{2.13}$$

the field equations can be rewritten as:

$$\dot{w} = u, \tag{2.14}$$

$$\dot{u} + 3uv - \frac{\alpha}{2} \frac{k m_{Pl}^2}{H_0^2} w^{-(\alpha+1)} = 0, \tag{2.15}$$

$$\dot{v} + \frac{3}{2} v^2 + \frac{u^2}{8} - \frac{1}{8} \frac{k m_{Pl}^2}{H_0^2} w^{-\alpha} = 0. \tag{2.16}$$

We numerically evolve the fields using the initial conditions $u(t_i) = 0$, $v(t_i) \gg 1$ as before. For fixed values of the model parameters α and k, the choice of the initial field value $w(t_i)$ determines the cosmological parameters $\Omega_{\phi 0}$ and $H_0 t_0$. Alternatively, we can keep α and $w(t_i)$ fixed and use $\Omega_{m0} = 1 - \Omega_{\phi 0}$ rather than k as our free parameter; we shall follow this approach below.

As an example, Fig. 4 shows the evolution for $\alpha = 5$, $w(t_i) = 3$, and $\Omega_{m0} = 0.2$. For this model $H_0 t_0 = 0.92$, larger than the value $H_0 t_0 = 0.85$ obtained in an open model with the same value of Ω_{m0}. In the next section, we shall see that this choice of parameters and initial conditions is consistent with the high-z SNe Ia constraints.

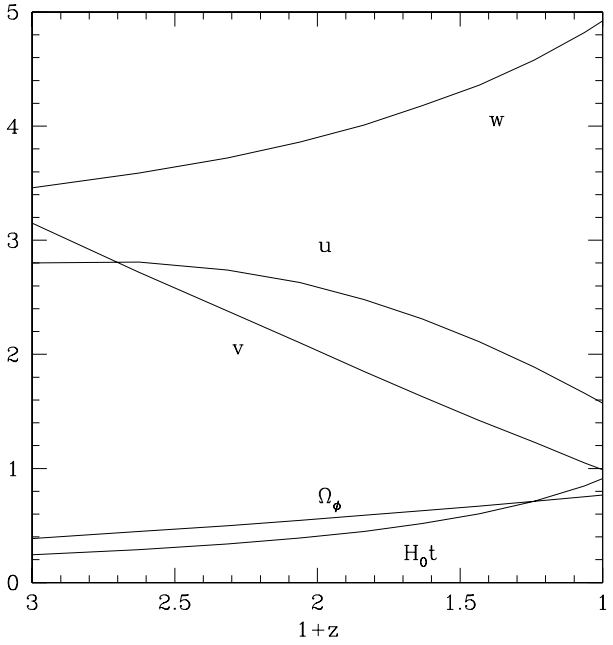

FIG. 4. Evolution of the variables u, v, w, Ω_ϕ, and $H_0 t_0$ for a power-law potential with $\alpha = 5$, $w(t_i) = 3$, and $\Omega_{m0} = 0.2$.

C. Exponential potentials

In this case the scalar field potential has the functional form,

$$V(\phi) = V_0 \, e^{-\phi/f}, \tag{2.17}$$

with positive constants V_0 and f. Scalar fields with an exponential potential have been investigated in the context of power-law inflationary models [25]. Cosmological consequences of scalar fields with exponential potentials dominating the dynamics of the Universe at late times were analyzed in [12,26].

Again introducing dimensionless variables,

$$u = \frac{1}{H_0 f}\frac{d\phi}{dt}, \; v = \frac{H}{H_0} \quad \text{and} \quad w = \frac{\phi}{f} - \ln\left(\frac{V_0}{m_{Pl}^2 H_0^2}\right), \tag{2.18}$$

the field equations become

$$\dot{w} = u, \tag{2.19}$$

$$\dot{u} + 3uv - 8\pi\beta \, e^{-w} = 0, \tag{2.20}$$

$$\dot{v} + \frac{3}{2}v^2 + \frac{u^2}{4\beta} - 4\pi e^{-w} = 0, \tag{2.21}$$

where $\beta = m_{Pl}^2/8\pi f^2$. We numerically evolve the fields with the initial conditions $u(t_i) = 0$, $v(t_i) \gg 1$. The mass parameter β and the initial field value $w(t_i)$ determine the cosmological parameters Ω_{m0} and $H_0 t_0$. We note that V_0 is not a fundamental constant: as Eq.(2.18) shows, changing V_0 is equivalent to reescaling the scalar field ϕ.

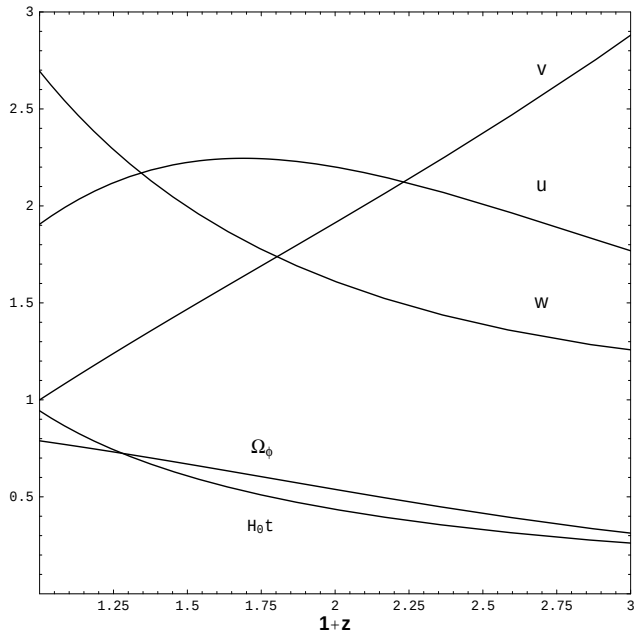

FIG. 5. Evolution of the variables u, v, w, Ω_ϕ, and H_0t with redshift in the exponential potential model with $w(t_i) = 1$ and $\ln\beta = 1$.

In Fig. 5, we show the evolution of the quantities u, v, w, $\Omega_\phi(t)$, and H_0t with redshift z for the parameter choice $\beta = 2.72$ and the initial condition $w(t_i) = 1$. For this case, we obtain $\Omega_{m0} = 0.21$ and $H_0t_0 = 0.94$; by comparison, in an open model with the same value of Ω_{m0}, we would have $H_0t_0 = 0.84$. In the next section we show that this choice of model parameters is consistent with the SNe Ia data.

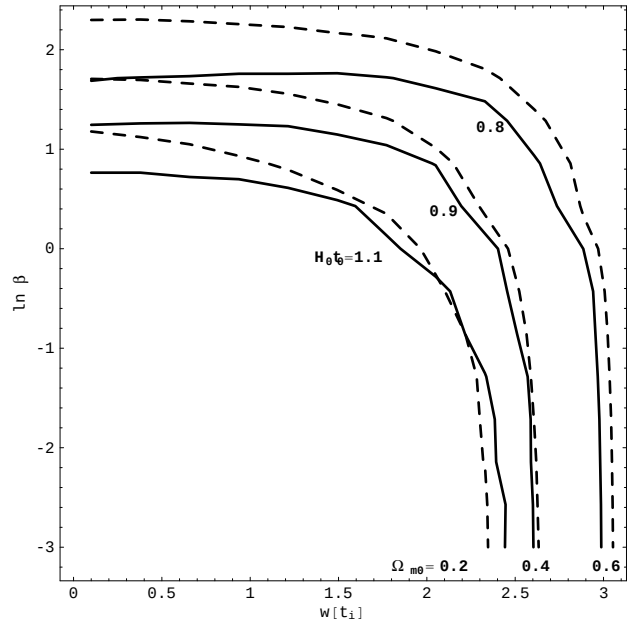

FIG. 6. Contours of constant Ω_{m0}(dashed curves) and H_0t_0 (solid) in the $\ln\beta - w(t_i)$ parameter space for exponential potentials.

In Fig.6 we show contours of constant Ω_{m0} (dashed curves) and H_0t_0 (solid) in the $\ln\beta - w(t_i)$ parameter space.

From the point of view of both large scale structure and age constraints, the most interesting region of the parameter space would seem to be the bottom right-hand portion of the figure, the locus of highest $H_0 t_0$ for fixed Ω_{mo}. However, as we shall see in the next section, the SNe Ia constraints practically exclude this region. We will show that for values of the mass parameter $\ln \beta \lesssim -2$, the SNe constraints imply $w(t_i) \gtrsim 3$; for these values of the parameters, however, $\Omega_{m0} \gtrsim 0.6$ and $H_0 t_0 \lesssim 0.8$.

III. CONSTRAINTS FROM HIGH-REDSHIFT TYPE IA SUPERNOVAE

A. The SNe observations

There are now two major ongoing programs to systematically discover high-redshift supernovae. In a recent report Perlmutter *et al.* [19] analyzed a first set of seven Type Ia SNe with redshifts $z = 0.35 - 0.46$ and obtained constraints on the cosmological parameters. Their preliminary result, $\Omega_\Lambda < 0.51$ at the 95% confidence level, strongly constrains models with a cosmological constant. In this section we use these data to constrain the scalar field cosmological models described in the preceding section.

The essential idea behind the technique is to apply the classical redshift-magnitude test to SNe Ia as standard candles. For a source of absolute magnitude M, the apparent bolometric magnitude $m(z)$ can be expressed as

$$m(z) = \mathcal{M} + 5 \log d_l, \tag{3.1}$$

where d_l is the luminosity distance in units of H_0^{-1}, and

$$\mathcal{M} = \mathrm{M} - 5 \log H_0 + 25 \tag{3.2}$$

is the "zero point" magnitude (or Hubble intercept magnitude), estimated from observations of low-redshift ($z < 0.1$) SNe Ia. The nearby supernovae data set used in [19] to determine $\mathcal{M}$ comprised those 18 SNe Ia discovered in the Calan/Tololo Supernovae Search [27] for which the first observations were made no later than 5 days after maximum.

Arising from the explosion of accreting white dwarfs, SNe Ia do not constitute a completely homogeneous class: there is significant dispersion in their absolute magnitudes at maximum light. However, it has been shown that SN Ia peak absolute magnitude is correlated with the rate at which the light curve subsequently declines [28]: brighter SNe Ia fade more slowly. The rate of decline can be quantified, e.g., by Δm_{15}, the B-magnitude decline in the first 15 days after maximum. For the Calan/Tololo sample, correction of the observed B-magnitudes using Δm_{15} reduced the dispersion in peak absolute magnitude from $\sigma_{M_B,corr} = 0.26$ to 0.17. A similar procedure applied to the Perlmutter *et al.* sample achieved comparable results, reducing σ_M from 0.27 to 0.19 mag. The width-luminosity correlation has been developed with the light-curve shape method [29] and further refined with the use of multiple pass bands [30].

In our computations we follow [19] and use the corrected B-magnitude intercept at $\Delta m_{15} = 1.1$ mag, $\mathcal{M}_{B,corr}^{\{1.1\}} = -3.32 \pm 0.05$. Of the 7 SNe Ia in the high-redshift sample, we consider only those 5 that satisfy $0.8 < \Delta m_{15} < 1.5$, corresponding to the range of values covered by the calibrating set of 18 low-redshift supernovae. To construct the χ^2 values, we used the outer error bars of the Ref. [19] data points, obtained by adding in quadrature the error bars of $m_{B,corr}$ (the apparent B-magnitudes after width-luminosity correction) to $\sigma_{M_B,corr}$.

B. Results

1. The PNGB model

We calculate the apparent magnitude-redshift relation for a grid of PNGB models in the $f - M$ parameter space and compare with the high-redshift SNe Ia observations. In Fig. 7 we show the corresponding 95%, 90%, and 68% confidence level bounds on the parameters f and M. As for Figs. 2 and 3, these limits apply to models with the initial condition $w(t_i) = 1.5$; for other choices, the bounding contours would shift by small amounts in the $f - M$ plane.

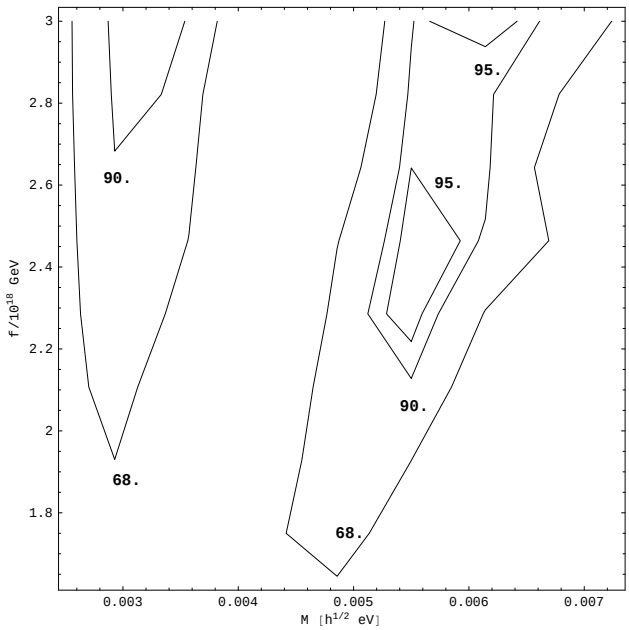

FIG. 7. Limits on the $f - M$ parameter space of PNGB models from the first set of high-redshift SNe Ia, for $w(t_i) = 1.5$; the lowest and highest contours are $1-$ and $2-\sigma$ limits.

Note the existence of two excluded regions of parameter space, one at the left and the other in the right portion of the figure. To understand the meaning of these regions, consider three cases with fixed $f = 3 \times 10^{18}$ GeV and varying $M = 0.003$, 0.0045, and 0.006 eV. The first and third choices are excluded by the SNe data while the second is allowed. With increasing M, the corresponding values of $\Omega_{\phi 0}$ and $H_0 t_0$ are (0.83, 1.07), (0.96, 1.11), and (0.80, 0.93). In all three cases, the Universe is ϕ-dominated ($\Omega_\phi \gg \Omega_m$) for $z \lesssim 1$, but the evolution differs markedly between them. To see this, in Fig. 8 we show the effective adiabatic index of the scalar field, $\gamma_\phi(t)$, as a function of redshift for the three cases.

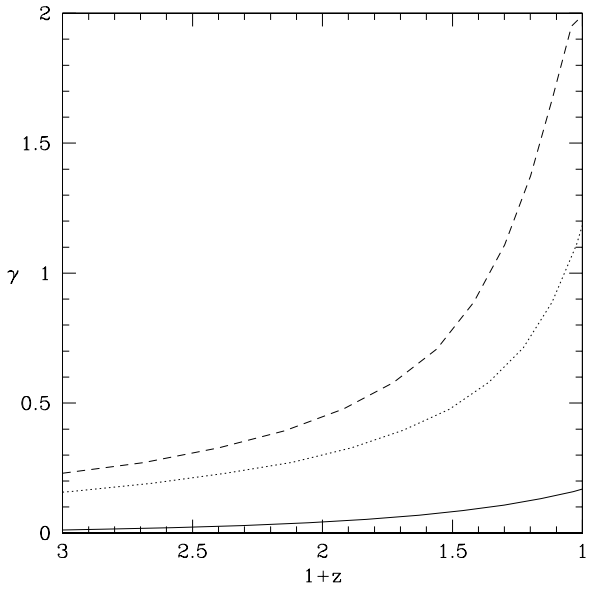

FIG. 8. Evolution of the equation of state parameter γ_ϕ with redshift for three PNGB models with $f = 3 \times 10^{18}$ GeV and $w(t_i) = 1.5$: $M = 0.003$ eV (solid), $M = 0.0045$ (dotted), and $M = 0.006$ eV (dashed).

For the first case, $M = 0.003$ eV, γ_ϕ remains close to zero throughout the evolution; in this case, the low value of M implies that the effective scalar mass $m_\phi \lesssim 3H_0$, and the nearly static scalar field behaves approximately like a cosmological constant until the present epoch. As a result, the redshift-magnitude relation for this case will be similar to that of a Λ model with $\Omega_\Lambda \simeq 0.83$, which is excluded by the SNe Ia data. In the second case, $M = 0.0045$ eV, the evolution of γ_ϕ is more pronounced, increasing from $\gamma \sim 0.3$ at $z = 1$ to $\gamma \sim 1.2$ at $z = 0$. At the moderate redshifts probed by the current SNe observations, $z \lesssim 0.4$, the effective equation of state in this case does not differ drastically from that of the Einstein-de Sitter model ($\gamma = 1$), which is consistent with the SNe data. In the third case, with $M = 0.006$ eV, γ increases to large values at recent epochs, again producing a distance-redshift relation appreciably different from that of the Einstein-de Sitter model.

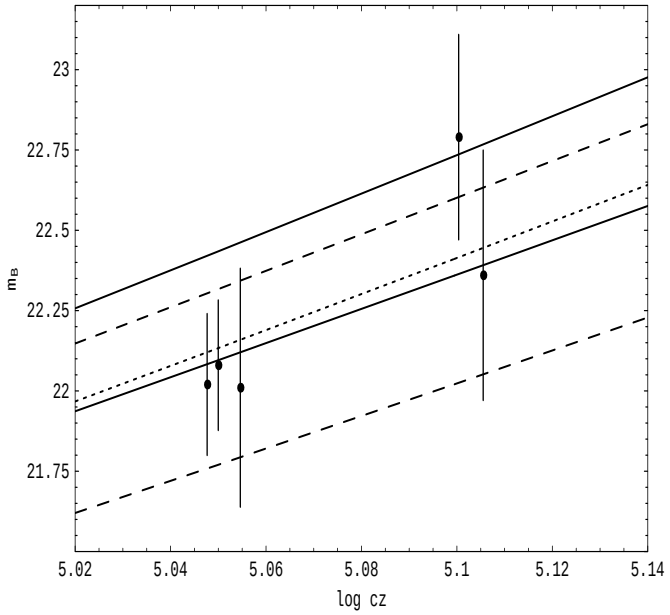

FIG. 9. Apparent magnitude vs. redshift relation is shown for the 3 PNGB models corresponding to Fig.8: $M = 0.003$ eV (top solid line); 0.0045 eV (middle dotted line); 0.006 eV (bottom dashed line). For comparison, we also show the prediction for the standard $\Omega_m = 1$ Einstein-de Sitter model (middle solid line), and for the Λ model at the 95 % C.L. limit, $\Omega_\Lambda = 0.51$ (top short dashed line). The data points are the light curve-corrected data for the 5 high-z SNe Ia.

In Fig. 9 we display the apparent magnitude-redshift relation for these three cases along with the corrected magnitudes for the five high-redshift SNe Ia used in this analysis. For comparison we also show the prediction of the Einstein-de Sitter model and the Λ model at the 95% C.L. limit. The $M = 0.003$ eV case is ruled out because, as in the Λ model, SNe at fixed redshift should be brighter than observed; in the $M = 0.006$ eV case, sources are too faint.

Thus, the behavior of the effective scalar equation of state provides a qualitative understanding of the topology of the exclusion regions in Fig. 7. By comparing Fig. 7 with Figs. 2 and 3, we see that the allowed region of parameter space includes models with low Ω_{m0} and a relatively high value of $H_0 t_0$ (as compared with open models with the same Ω_{m0}). For example, for $f = 2.0 \times 10^{18}$ GeV and $M = 0.0035$ eV, parameter values consistent with the SNe data, we have $\Omega_{m0} = 0.25$ and $H_0 t_0 = 0.92$. An open model with the same value of Ω_{m0} would correspond to $H_0 t_0 = 0.83$. A particular interesting region of parameter space is the area around $f = 1.8 \times 10^{27}$ eV and $M = 0.003$ eV, in the protuberance of Fig. 3. For these parameter values, the age is relatively high, $H_0 t_0 = 0.87$, the magnitude-redshift relation is consistent with the SNe data, and the present matter density is $\Omega_{m0} = 0.38$. With CDM and normalized to COBE, this model predicts a large-scale power spectrum consistent with the galaxy clustering data as well [16].

2. Power-Law Potentials

As noted above, for fixed $w(t_i)$, the model parameters for the power-law potentials can be taken to be Ω_{m0} and α. In Fig.10 we show the 95%, 90%, and 68% C. L. limits from the SNe Ia data on the parameter space for these models. As in Fig. 4, we have fixed $w(t_i) = 3$. We also display the contours of constant $H_0 t_0$. For $\Omega_{m0} = 0.2$, 0.3, and 0.4, the $1 - \sigma$ SNe limits are $\alpha \geq 4.45$, 4.07, and 3.6, respectively, and the corresponding upper limits on $H_0 t_0$ are 0.95,

0.91, and 0.86.

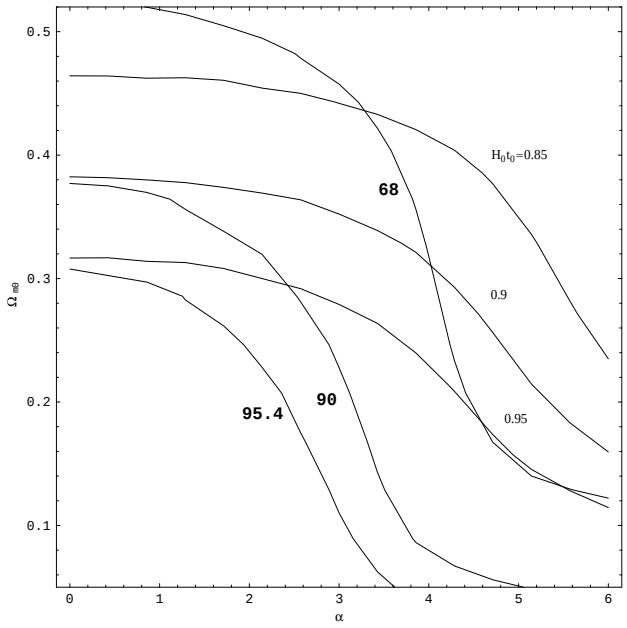

FIG. 10. Contours for the $1-\sigma$, 90% C.L., and $2-\sigma$ SNe Ia limits in the $\alpha - \Omega_{m0}$ parameter space for power-law potentials. Also shown are contours of constant $H_0 t_0 = 0.85$, 0.9, and 0.95.

3. Exponential Potentials

In Fig.11 we show the 95.4%, 90%, and 68% C. L. SNe Ia limits on the $\ln\beta - w(t_i)$ parameter space for the exponential potential models. As noted in the discussion of Fig. 6, the region in the bottom right portion of the figure is not cosmologically interesting: for $w(t_i) \gtrsim 2.9$, as required at $1-\sigma$ by the SNe data, Fig. 6 indicates that $\Omega_{m0} \gtrsim 0.55$, substantially larger than that observed on cluster scales. Of more interest is a region at the upper left of Figs. 6 and 11, where $w(t_i) \lesssim 1.5$ and $0.9 \lesssim \ln\beta \lesssim 1.8$. This region is allowed by the SNe data, yields $H_0 t_0 \sim 0.9 \pm 0.1$, and corresponds to $\Omega_{m0} \simeq 0.3 - 0.4$.

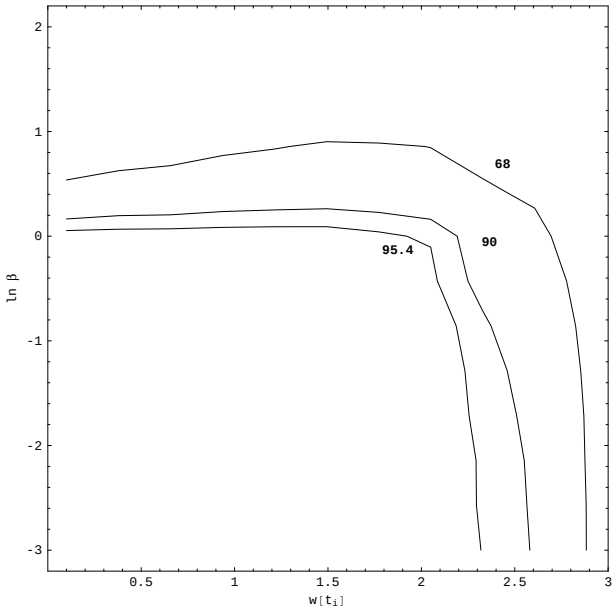

FIG. 11. SNe Ia constraints on the parameter space of exponential potential models.

IV. CONCLUSIONS

We have studied the observational implications of cosmological models in which a classical scalar field dominates the energy density of the Universe at recent epochs. The motivation for introducing these fields was to provide a dynamical model for the cosmological constant, which is favored by observations but whose origin remains obscure. These three examples were chosen from the literature in order to illustrate the range of expected behavior in scalar field models. To date, the most stringent observational constraint on the cosmological constant comes from recent observations of distant Type Ia supernovae, $\Omega_\Lambda < 0.51$ at $2-\sigma$. We have extended this constraint to the scalar field "dynamical" Λ models. Since the effective equation of state of an evolving scalar field differs from that of a conventional cosmological constant, there are regions of parameter space for which the model predictions are consistent with the SNe observations, even at relatively high values of Ω_ϕ. In particular, there are viable scalar field models with $\Omega_{m0} \simeq 0.2 - 0.3$, consistent with cluster observations, and which are spatially flat, consistent with the predictions of inflation. We close by stressing that the high-redshift SNe results are preliminary, based on a new technique applied to a very small sample. The on-going SNe searches are continuing to discover SNe Ia; as the sample grows and the systematic effects become better studied, the constraints on cosmological parameters, and on the kinds of cosmological models studied here, should become more robust.

ACKNOWLEDGMENTS

We thank Saul Perlmutter for helpful discussions. This research was supported in part by the DOE and NASA grant NAG5-2788 at Fermilab and by the Brazilian agency CNPq.

---

[1] R. Carlberg, et al., Astrophys. J. **462**, 32 (1996).
[2] A. Dekel, D. Burstein, and S. White, in *Critical Dialogues in Cosmology*, ed. N. Turok (World Scientific, 1997), astro-ph/9611108.
[3] W. Freedman, in *Proc. of the 18th Texas Symposium on Relativistic Astrophysics*, eds. A. Olinto, J. Frieman, and D. Schramm (World Scientific, in press), astro-ph/9706072.
[4] B. Chaboyer, P. Demarque, P. J. Kernan, and L. M. Krauss, Science **271**, 957 (1996).
[5] B. Chaboyer, P. Demarque, P. J. Kernan, and L. M. Krauss, astro-ph/9706128.
[6] G. Efstathiou, S. Maddox, and W. Sutherland, Nature (London) **348**, 705 (1990); L. Kofman, N. Gnedin, and N. Bahcall, Astrophys. J. **413**, 1 (1993).
[7] J. A. Peacock and S. J. Dodds, Mon. Not. R. Astron. Soc. **267**, 1020 (1994).
[8] C. S. Kochanek, Ap. J. **466**, 638 (1996) and references therein. This limit is, however, subject to possible systematic errors, including extinction by dust in the lensing galaxy. See, e.g., S. Malhotra, J. E. Rhoads, and E. L. Turner, Mon. Not. Roy. Astron. Soc., in press (1997), astro-ph/9610233.
[9] A. Klypin, J. Primack, and J. Holtzman, Ap. J. **466**, 13 (1996).
[10] M. Ozer and M. O. Taha, Nucl. Phys. **B287**, 776 (1987); K. Freese, F. C. Adams, J. A. Frieman, and E. Mottola, Nucl. Phys. **287**, 797 (1987); W. Chen and Y. S. Wu, Phys. Rev. **D41**, 695 (1990); J. C. Carvalho, J. A. S. Lima, and I. Waga, Phys. Rev. **D46**, 2404 (1992); V. Silveira and I. Waga, Phys. Rev. **D50**, 4890 (1994).
[11] P. J. E. Peebles and B. Ratra, Ap. J., **325**, L17 (1988).
[12] B. Ratra and P. J. E. Peebles, Phys. Rev. **D37**, 3406 (1988).
[13] J. A. Frieman, C. T. Hill, A. Stebbins, and I. Waga, Phys. Rev. Lett. **75**, 2077 (1995).
[14] B. Ratra and A. Quillen, Mon. Not. R. Astron. Soc. **259**, 738 (1992).
[15] L. F. Bloomfield Torres and I. Waga, Mon. Not. R. Astron. Soc. **279**, 712 (1996).
[16] K. Coble, S. Dodelson, and J. A. Frieman, Phys. Rev. **D55**, 1851 (1997).
[17] R. R. Caldwell, R. Dave, and P. J. Steinhardt, astro-ph/9708069.
[18] P. T. P. Viana and A. R. Liddle, astro-ph/9708247.
[19] S. Perlmutter *et al.*, Ap. J. **483**, 565 (1997).
[20] B. Schmidt, B., etal. in *Thermonuclear Supernovae*, eds. R. Ruiz-Lapuente, R. Canal, and J. Isern (Dordrecht: Kluwer, 1997).
[21] P. J. Steinhardt, Nature **382**, 768 (1996); M. Turner and M. White, astro-ph/9701138; V. Silveira and I. Waga, astro-ph/9703185.
[22] J. Frieman, C. Hill, and R. Watkins, Phys. Rev. D **46**, 1226 (1992).

[23] M. Fukugita and T. Yanagida, preprint YITP/K-1098 (1995).
[24] W. Kinney and A. Riotto, Fermilab-Pub-97-090-A (hep-ph/9704388) and references therein.
[25] See, e.g., L. F. Lucchin and S. Matarrese, Phys. Rev. **D32**, 217, (1985); J. J. Halliwell, Phys. Lett. **B 185**, 341, (1987); A. B. Burd and J. D. Barrow, Nucl. Phys **B308**, 929 (1988); A. R. Liddle, Phys. Lett. **B 220**, 502 (1989).
[26] V. Sahni, H. Feldman, and A. Stebbins, Ap. J. **385**, 1 (1992).
[27] M. Hamuy *et al.*, Astron. J. **109**, 1 (1995). M. Hamuy *et al.*, Astron. J. **112**, 2391 (1996).
[28] M. M. Phillips, Ap. J. **413**, L105 (1993).
[29] A. G. Riess, W. H. Press, and R. P. Kirshner, Ap. J. **438**, L17 (1995).
[30] A. G. Riess, W. H. Press, and R. P. Kirshner, Ap. J. **473**, 88 (1996).